

# Multi-types of Instability Process of Periodic Orbits in Nonlinear Chains

Weicheng Fu<sup>1,2,3,\*</sup>, Zhen Wang<sup>4</sup>, Yong Zhang<sup>5,3,†</sup> and Hong Zhao<sup>5,3</sup>

<sup>1</sup> Department of Physics, Tianshui Normal University, Tianshui 741000, Gansu, China

<sup>2</sup> Key Laboratory of Atomic and Molecular Physics & Functional Material of Gansu Province, College of Physics and Electronic Engineering, Northwest Normal University, Lanzhou 730070, China

<sup>3</sup> Lanzhou Center for Theoretical Physics, Key Laboratory of Theoretical Physics of Gansu Province, and Key Laboratory of Quantum Theory and Applications of MoE, Lanzhou University, Lanzhou, Gansu 730000, China

<sup>4</sup> CAS Key Laboratory of Theoretical Physics and Institute of Theoretical Physics, Chinese Academy of Sciences, Beijing 100190, China

<sup>5</sup> Department of Physics, Xiamen University, Xiamen 361005, Fujian, China

(Dated: January 29, 2025)

Nonlinear normal modes are periodic orbits that survive in nonlinear many-body Hamiltonian systems, and their instability plays a key role in the system's relaxation dynamics. We investigate here the instability of the  $\pi/3$ -mode in the Fermi-Pasta-Ulam-Tsingou- $\alpha$  chain with fixed boundary conditions. We find that three types of bifurcations—period-doubling, tangent, and Hopf bifurcations—coexist in this system, each driving instability at specific reduced wave-number  $\tilde{k}$ . Our analysis reveals a universal scaling law for the instability time  $\mathcal{T} \propto (\lambda - \lambda_c)^{-1/2}$ , independent of bifurcation types and models, where the critical perturbation strength  $\lambda_c$  depends on  $\tilde{k}$  via  $\lambda_c \propto (\tilde{k} - \tilde{k}_c)$ , with  $\tilde{k}_c$  varying across bifurcations. We also observe a double instability phenomenon for certain system sizes. These results provide new insights into the relaxation and thermalization dynamics in many-body systems, with broad implications for nonlinear and non-equilibrium statistical physics.

*Introduction*—Conservation laws govern the relaxation and transport dynamics of many-body Hamiltonian systems [1–6]. When the number of conserved quantities equals that of degrees of freedom, the system is integrable, resulting in non-thermalization and ballistic transport behavior [7–11]. Under small perturbations, most conserved quantities are destroyed, yet some persist according to the Kolmogorov-Arnold-Moser theorem [12], as exemplified by the Fermi-Pasta-Ulam-Tsingou (FPUT) recurrence [13–15], which arises from  $q$ -breathers [16–19] or  $q$ -tori [20]. The breaking of invariant tori (i.e., periodic orbits)—whether, when, and how it occurs—has a critical effect on the relaxation properties of a system. The related subject remains an active research area, including studies on Bose gases [21–23], nonlinear phononic [24] and photonic systems [25, 26], and other quantum systems [27–29].

Nonlinear normal modes (NNMs) act as special periodic orbits, and their instability dynamics significantly influence the system's relaxation and thermalization behavior [30–36]. Extensive studies have shown that NNMs undergo bifurcations and become unstable when the perturbation strength  $\lambda$  exceeds a critical threshold  $\lambda_c$  [37–45]. For instance, previous work demonstrated that NNMs in the FPUT- $\beta$  model destabilize via a period-doubling bifurcation, while in the Bose-Einstein condensation model, they exhibit a tangent bifurcation [42].

In this work, we study the instability dynamics of the  $\pi/3$ -mode in the FPUT- $\alpha$  model with fixed boundary

conditions. We show that three types of bifurcations—period-doubling, tangent, and Hopf—coexist in the instability dynamics, providing valuable insights into the relaxation and thermalization processes in many-body Hamiltonian systems. The key to revealing this coexistence lies in analyzing the error evolution equation in the *reduced wave-number*  $\tilde{k}$  space, which enables a more comprehensive exploration of the parameter space and uncovers this richer, previously unobserved phenomenon. Additionally, both Floquet theory and numerical simulations consistently show that the instability time  $\mathcal{T}$  follows a critical exponent of  $1/2$ , i.e.,  $\mathcal{T} \propto (\lambda - \lambda_c)^{-1/2}$ , independent of the bifurcation type, NNM's wave-number, or the specific model. We also find that  $\lambda_c \propto (\tilde{k} - \tilde{k}_c)$ , with  $\tilde{k}_c = 0$  for the Hopf bifurcation and  $\tilde{k}_c = \frac{2}{\pi} \arcsin\left(\frac{\sqrt{3}}{4}\right)$  for the period-doubling bifurcation. Furthermore, we observe a double instability phenomenon in the destabilization dynamics of  $\pi/3$ -mode at certain system sizes, which implies that larger perturbations do not always accelerate thermalization.

*The Model*—The FPUT- $\alpha$  chain consists of  $N$  particles of unit mass interacting with their nearest neighbors, and its Hamiltonian reads:

$$H = \sum_{j=1}^N \left[ \frac{p_j^2}{2} + \frac{(x_j - x_{j-1})^2}{2} + \frac{\alpha}{3} (x_j - x_{j-1})^3 \right], \quad (1)$$

where  $p_j$  and  $x_j$  are, respectively, the momentum and displacement from the equilibrium position of the  $j$ -th particle. The parameter  $\alpha$  is the nonlinear coupling strength, which controls the perturbation strength  $\lambda = \alpha^2 \varepsilon$  [46], with  $\varepsilon$  being the energy per particle.

\* fuweicheng@tsnu.edu.cn

† yzhang75@xmu.edu.cn

For convenience,  $x_j$  is represented by normal modes:

$$x_j(t) = \sqrt{\frac{2}{N}} \sum_{k=1}^{N-1} Q_k(t) \sin\left(\frac{jk\pi}{N}\right), \quad (2)$$

for fixed boundary conditions  $x_0 = p_0 = x_N = p_N = 0$ , where there are  $N - 1$  moving particles. Here,  $Q_k$  represents the amplitude of the  $k$ -th normal mode.

By combining Eqs. (1) and (2), we obtain the equations of motion for the normal modes:

$$\ddot{Q}_k = -\omega_k^2 Q_k - \frac{\alpha}{\sqrt{2N}} \sum_{k_2, k_3} \omega_k \omega_{k_2} \omega_{k_3} C_{k, k_2, k_3} Q_{k_2} Q_{k_3}, \quad (3)$$

where  $\omega_k$  is the frequency of the  $k$ -th mode, given by

$$\omega_k = 2 \sin\left(\frac{\pi k}{2N}\right) = 2 \sin\left(\frac{\tilde{k}\pi}{2}\right), \quad 1 \leq k \leq N - 1, \quad (4)$$

and  $\tilde{k} = k/N$  is the *reduced wave-number*.  $C_{k_1, k_2, k_3}$  represents the selection rules [36]:

$$C_{k_1, k_2, k_3} = \delta_{k_1 - k_2 - k_3, 0} + \delta_{k_1 - k_2 + k_3, 0} + \delta_{k_1 + k_2 - k_3, 0} - \delta_{k_1 + k_2 + k_3, 2N}, \quad (5)$$

where  $\delta$  is the Kronecker delta function.

*The solution of  $\pi/3$ -mode*—Suppose only the  $\pi/3$ -mode (i.e.,  $k = 2N/3$ , and  $N$  is an integer multiple of 3) is initially excited, while all other modes remain frozen. Under this condition, Eq. (3) reduces to

$$\ddot{Q}_{\pi/3} = -3Q_{\pi/3} + \frac{3\sqrt{3}\alpha}{\sqrt{2N}} Q_{\pi/3}^2, \quad (6)$$

whose solution can be expressed in terms of the Jacobi elliptic cosine function  $\text{cn}$  as

$$Q_{\pi/3} = a + b \text{cn}^2[\Omega t, m], \quad (7)$$

where  $a = \frac{\theta - 1 + 2m}{\alpha\theta} \sqrt{\frac{N}{6}}$ ,  $b = -\frac{3m}{\theta} \sqrt{\frac{N}{6}}$ , and  $\Omega^2 = \frac{3}{4\theta}$ , in which  $\theta = \sqrt{m^2 - m + 1}$ , and the parameter  $m = \kappa^2$  is defined by the elliptic modulus  $\kappa$ , which is related the *perturbation strength* by

$$\lambda = \frac{N}{N-1} \left[ \frac{1}{6} - \frac{(m+1)(2m^2 - 5m + 2)}{12(m^2 - m + 1)^{3/2}} \right]. \quad (8)$$

Note that the period  $T$  of  $Q_{\pi/3}$  is half the period of the  $\text{cn}$ , given by  $T = 2K(m)/\Omega$ , where  $K(m)$  is the complete elliptic integral of the first kind (see Sec. A in the Supplemental Material [47] for the solution derivation).

*Linear stability analysis*—Assuming only the  $\pi/3$ -mode is excited, let  $\mathcal{Q}_k$  represent the error in mode  $Q_k$ . From Eq. (3), we derive the equation of motion for  $\mathcal{Q}_k$ :

$$\ddot{\mathcal{Q}}_k = -\omega_k^2 \mathcal{Q}_k - \alpha \omega_k \sqrt{\frac{6}{N}} Q_{\pi/3} \sum_{k_3} \omega_{k_3} C_{k, \frac{2N}{3}, k_3} \mathcal{Q}_{k_3}, \quad (9)$$

where  $C_{k, 2N/3, k_3}$  is nonzero only when  $k_3 = k - 2N/3$ ,  $k_3 = 2N/3 - k$ ,  $k_3 = k + 2N/3$ , or  $k_3 = 4N/3 - k$ , which results in the following three-mode coupled equations:

$$\begin{cases} \ddot{\mathcal{Q}}_k &= -\omega_k^2 \mathcal{Q}_k - \Lambda \omega_k (\omega_{k_2} \mathcal{Q}_{k_2} + \omega_{k_3} \mathcal{Q}_{k_3}), \\ \ddot{\mathcal{Q}}_{k_2} &= -\omega_{k_2}^2 \mathcal{Q}_{k_2} - \Lambda \omega_{k_2} (\omega_k \mathcal{Q}_k - \omega_{k_3} \mathcal{Q}_{k_3}), \\ \ddot{\mathcal{Q}}_{k_3} &= -\omega_{k_3}^2 \mathcal{Q}_{k_3} - \Lambda \omega_{k_3} (\omega_k \mathcal{Q}_k - \omega_{k_2} \mathcal{Q}_{k_2}), \end{cases} \quad (10)$$

where  $k \in (0, N/3)$ ,  $k_2 = 2N/3 - k \in (N/3, 2N/3)$ , and  $k_3 = 2N/3 + k \in (2N/3, N)$ ; and

$$\Lambda = \alpha \sqrt{\frac{6}{N}} Q_{\pi/3} = \left(1 - \frac{1-2m}{\theta}\right) - \frac{3m}{\theta} \text{cn}^2[\Omega t, m], \quad (11)$$

which is a periodic function *independent of system size* (see Sec. B in the Supplemental Material [47] for details).

Defining  $\mathbf{W} = [\mathcal{Q}_k \ \dot{\mathcal{Q}}_k \ \mathcal{Q}_{k_2} \ \dot{\mathcal{Q}}_{k_2} \ \mathcal{Q}_{k_3} \ \dot{\mathcal{Q}}_{k_3}]^T$ , then Eq. (10) can be further rewritten as:

$$\dot{\mathbf{W}} = \mathbf{A}(t)\mathbf{W}, \quad (12)$$

where the coefficient matrix

$$\mathbf{A}(t) = \begin{bmatrix} 0 & 1 & 0 & 0 & 0 & 0 \\ -\omega_k^2 & 0 & -\Lambda \omega_k \omega_{k_2} & 0 & -\Lambda \omega_k \omega_{k_3} & 0 \\ 0 & 0 & 0 & 1 & 0 & 0 \\ -\Lambda \omega_k \omega_{k_2} & 0 & -\omega_{k_2}^2 & 0 & \Lambda \omega_{k_2} \omega_{k_3} & 0 \\ 0 & 0 & 0 & 0 & 0 & 1 \\ -\Lambda \omega_k \omega_{k_3} & 0 & \Lambda \omega_{k_2} \omega_{k_3} & 0 & -\omega_{k_3}^2 & 0 \end{bmatrix} \quad (13)$$

with the period of  $T$ .

According to Floquet theory [48], the solution of Eq. (12) has the following form:

$$\mathbf{W}(t) \sim e^{\mu t} \mathbf{S}(t), \quad (14)$$

where  $\mathbf{S}(t)$  is periodic with period  $T$ , and  $\mu$  is the Floquet exponent, which may be complex.

The principal fundamental matrix  $\mathbf{X}(t)$  for the system (12) is given by

$$\dot{\mathbf{X}}(t) = \mathbf{A}(t)\mathbf{X}(t). \quad (15)$$

with the initial condition  $\mathbf{X}(0) = \mathbf{I}$  (i.e. identity matrix) [48]. The eigenvalues  $\rho_j$ s of  $\mathbf{X}(T)$  are known as the Floquet multipliers. The Floquet exponents  $\mu_j$ s are given by  $\mu_j = \ln(\rho_j)/T$ . If  $|\rho_j| \leq 1$  (i.e.,  $\Re(\mu_j) \leq 0$ ) for all  $j \in [1, 6]$ , the system is stable. Conversely, if any  $|\rho_j| > 1$  (i.e.,  $\Re(\mu_j) > 0$ ), the system becomes unstable, since the error will increase exponentially, see expression (14), and the instability time  $\mathcal{T}$  can be estimated as:

$$\mathcal{T} \propto 1/\Re(\mu_j). \quad (16)$$

In practice, given  $N$ , we select a mode  $k \in [1, N/3)$ , integrate Eq. (15) to obtain  $\mathbf{X}(T)$ . The instability threshold  $\lambda_{c,k}$  for the  $k$ th mode is determined by solving  $D = 0$  [here  $D$  represents the discriminant of the characteristic polynomial of  $\mathbf{X}(T)$ ].  $D(\lambda_{c,k}) = 0$  means that a pair of  $\rho_j$ s collide on the unit circle and will soon leave it (see

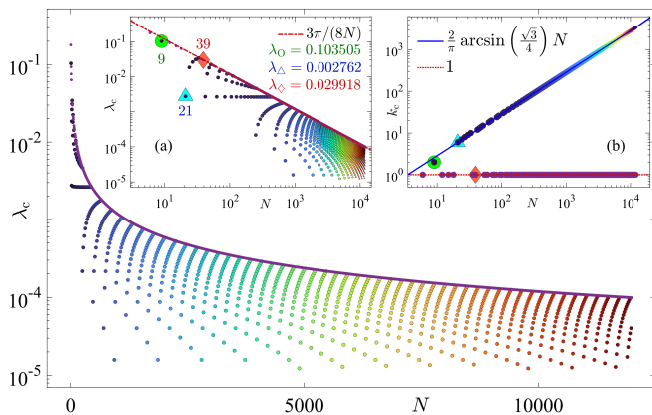


FIG. 1. Dependence of  $\lambda_c$  on  $N$ . Inset (a): Same as the main panel but in log-log scale, with the red dashed line as a reference. The  $\lambda$  with different subscripts corresponds to  $\lambda_c$  for the size indicated by the shape. Inset (b):  $k_c$  versus  $N$ .

Fig. 4). We define the critical threshold  $\lambda_c$  as the minimum value among  $\lambda_{c,k}$ , i.e.,  $\lambda_c = \min\{\lambda_{c,k}\}$ , above which the system becomes unstable. The corresponding mode index  $k_c$  identifies the first mode to lose stability. Next, we derive  $\tilde{k}_c$ .

In fact, given  $\tilde{k}$ ,  $m$  (or  $\lambda$ ) is the sole argument of  $\mathbf{X}(T)$ . On the other hand, one knows that the NNM is *linearly stable*, and, in general,  $\lambda_c$  will approach zero in the thermodynamic limit, i.e.,  $\lambda_c \rightarrow 0$  (viz.  $m \rightarrow 0$ ) as  $N \rightarrow \infty$ . Therefore, we reverse the approach: let  $m \rightarrow 0$ , then  $\text{cn}(\Omega t, m) \rightarrow \cos(\Omega t)$ , now, Eq. (15) depends only on  $N$ , or more precisely, on  $\tilde{k}$ , and the equation becomes solvable. Solving  $D(k_c) = 0$  will determine which mode become unstable first. If there is no solution for  $D(\tilde{k}_c) = 0$ , this implies that the assumption is invalid, meaning that, in the thermodynamic limit,  $\lambda_c$  is finite, not zero. Here, for  $m \rightarrow 0$ , we obtain

$$\tilde{k}_c = \frac{k_c}{N} = \begin{cases} 0, & \text{tangent or Hopf bifurcation;} \\ \frac{2}{\pi} \arcsin\left(\frac{\sqrt{3}}{4}\right), & \text{period-doubling,} \end{cases} \quad (17)$$

which implies that the mode  $k_c = 1$  or  $k_c = \lfloor N\tilde{k}_c \rfloor$  will lose stability first, where  $\lfloor \cdot \rfloor$  denotes the integer part (see Sec. C in the Supplemental Material [47] for details, especially discussion for bifurcation's type).

Although an *approximate solution* to the Eq. (15) can be obtained using perturbation theory [43], the resulting expression is too lengthy to readily offer clear physical intuition. To gain better insight, we instead solve the equation numerically using the embedded Runge-Kutta-Nystrom algorithm of order 12(10) [49] and present the results in graphical form.

*Numerical solutions*—First, we calculate  $\lambda_c$  and  $k_c$  for different system sizes  $N$ , as shown in Fig. 1, where the scatter points represents the value of  $k_c$  associated with  $\lambda_c$ , revealing a rich structure. Inset (a) presents the same results as the main panel, but in log-log scale. Inset (b) shows the dependence of  $k_c$  on  $N$ , where two distinct

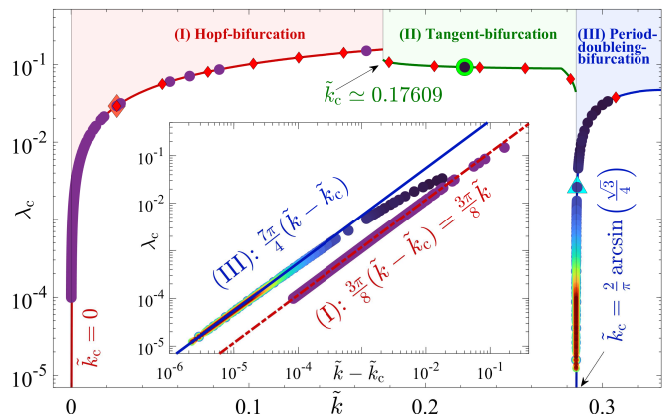


FIG. 2. Dependence of  $\lambda_c$  on  $\tilde{k}$ . The red diamonds represent  $\lambda_{c,k}$  for  $N = 39$ , with  $k \in [1, 12]$ . Inset: Same as the main panel [regions (I) and (III)], but with the horizontal axis replaced by  $(\tilde{k} - \tilde{k}_c)$ . Straight lines are shown for reference.

classes are clearly observed. One corresponds to  $k_c = 1$ , and the other to  $k_c = \lfloor \frac{2N}{\pi} \arcsin(\frac{\sqrt{3}}{4}) \rfloor$ , confirming the result in Eq. (17). We also find that  $\lambda_c \propto N^{-1}$  when  $k_c = 1$ , as indicated by the red dashed line in Inset (a). In terms of the reduced wave-number, it suggests  $\lambda_c \propto \tilde{k}$ .

Figure 2 shows  $\lambda_c$  as a function of  $\tilde{k}$ . The seemingly irregular data from Fig. 1 are now clearly organized into three distinct curves. The solid curves are obtained by solving Eq. (15) for  $\tilde{k}$ , which is treated as continuously varying in the range  $[0, 1/3]$ , ignoring the system's discreteness and its constraints on  $\tilde{k}$  [50]. The discrete results in Fig. 1 are rescaled by  $(1 - 1/N)$  to facilitate comparison with the solid curve, see circles. The solid curve exhibits discontinuities, dividing  $[0, 1/3]$  into three regions, which, from left to right, orderly correspond the Hopf bifurcation (I), tangent bifurcation (II) and period-doubling bifurcation (III). Clearly, region (II) corresponds to a finite  $\lambda_c$ , and  $\lambda_c \in (0.044, 0.116)$ . In our calculated range of  $N \in [6, 12000]$ , only the  $\lambda_c$  of  $N = 9$  locates in this region. Moreover, we see that  $\tilde{k}_c = 0$  for region (I), and  $\tilde{k}_c = \frac{2}{\pi} \arcsin(\frac{\sqrt{3}}{4})$  for region (III), which agree well with Eq. (17). To observe the scaling behavior of  $\lambda_c$  as  $\tilde{k} \rightarrow \tilde{k}_c$  in these two regions, we present the dependence of  $\lambda_c$  on  $(\tilde{k} - \tilde{k}_c)$  in the inset. The best linear fit shows that  $\lambda_c$  approximately follows the relation:

$$\lambda_c \simeq \begin{cases} \frac{3\pi}{8}(\tilde{k} - \tilde{k}_c), & \text{(I) : } \tilde{k}_c = 0; \\ \frac{7\pi}{4}(\tilde{k} - \tilde{k}_c), & \text{(III) : } \tilde{k}_c = \frac{2}{\pi} \arcsin\left(\frac{\sqrt{3}}{4}\right), \end{cases} \quad (18)$$

when  $\tilde{k} \rightarrow \tilde{k}_c$ , refer to the lines in the inset.

For a given  $N$ ,  $\lambda_{c,k}$  follows the same pattern as described above, with  $k \in [1, N/3]$ . As shown by the red diamonds for  $N = 39$  in Fig. 2. Considering Eq. (4), it is concluded that different frequencies in the system correspond to different bifurcation types:  $\omega_k \in (0, 0.5462)$  for region (I),  $\omega_k \in [0.5462, 0.866)$  for region (II), and  $\omega_k \in [0.866, 1.7321)$  for region (III). This demonstrates

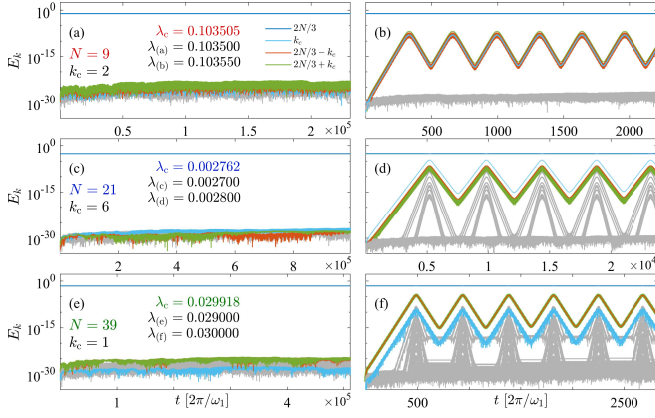


FIG. 3. Panels (a) and (b) show the evolution of  $E_k$  for  $N = 9$ , with  $\lambda_{(a)}$  and  $\lambda_{(b)}$  corresponding to the results in each panel, respectively. Panels (c) and (d) show results for  $N = 21$ , while panels (e) and (f) are for  $N = 39$ .

the strong predictive power of Fig. 2: for any  $N$ ,  $\lambda_{c,k}$  for  $\tilde{k}$  can be directly read from the plot. The minimum value corresponds to the system's  $\lambda_c$  and also identifies the type of bifurcation responsible for the instability.

We now validate the accuracy of Floquet's theory for threshold prediction through molecular dynamics simulations (MDS). Initially, the total energy is assigned to the  $2N/3$  mode, and the particles' positions are initialized using Eq. (2). The Hamiltonian canonical equations, derived from Eq. (1), are numerically evolved using the same algorithm, with the energy of modes,  $E_k(t)$  monitored, as shown in Fig. 3, where  $E_k$  defined as

$$E_k = \begin{cases} \frac{1}{2} (P_k^2 + \omega_k^2 Q_k^2), & k \neq 2N/3; \\ \frac{1}{2} (P_k^2 + 3Q_k^2) - \alpha \sqrt{\frac{3}{2N}} Q_k^3, & k = 2N/3, \end{cases} \quad (19)$$

here  $P_k = \partial H / \partial \dot{Q}_k$  is the canonical conjugate momentum. Clearly, for  $\lambda < \lambda_c$  (left three panels),  $E_{2N/3}(t)$  remains nearly constant, while the energy in other modes stays at zero (within numerical precision), indicating stability. In contrast, for  $\lambda > \lambda_c$  (right three panels), the error-coupled modes gain energy exponentially, and the energy exhibits quasi-periodic oscillations. However, the system eventually loses stability, as shown in Fig. 5(c). These numerical results are in good agreement with our theoretical predictions. We now proceed to examine the types of bifurcations.

Figures 4(a) and 4(b) show the dependence of  $\rho_j$  on  $\lambda$  for  $N = 9$ . A pair of  $\rho_j$ s first departs from the unit circle at  $+1$ , indicating a tangent bifurcation that destabilizes the system. The gray line corresponds to  $k = 1$ , where a pair of complex conjugate roots leaves the unit circle, signaling a Hopf bifurcation. Figure 4(c) shows  $\Re(\mu_j)$  as a function of  $\lambda$ , clearly illustrating that  $\lambda_c = \lambda_{c,2} < \lambda_{c,1}$ . Since  $\rho_j$ s are the roots of the characteristic polynomial of  $\mathbf{X}(T)$ , and  $\mu_j = \ln(\rho_j)/T$ , we have  $\Re(\mu_j(\lambda_c)) = 0$ . Thus, the lowest-order expansion of  $\Re(\mu_j)$  near  $\lambda_c$  is expected to scale as  $(\lambda - \lambda_c)^{1/2}$ , in agreement with the numerical

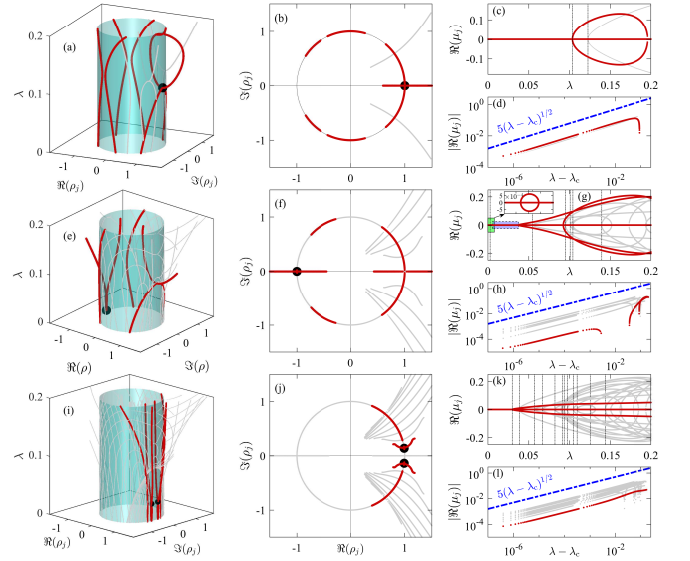


FIG. 4. Panels (a) and (b) show how  $\rho_j$ s move off the unit circle as  $\lambda$  increases for  $N = 9$ . The  $\rho_j$  that determines  $\lambda_c$  is plotted in red, while the others are in grey. Panel (c) shows  $\Re(\mu_j)$  versus  $\lambda$ , with the dashed line marking the transition from zero to non-zero. Panel (d) shows  $|\Re(\mu_j)|$  versus  $\lambda - \lambda_c$ , with a dashed blue reference line. Panels (e)-(h) and (i)-(l) replicate (a)-(d) for  $N = 21$  and  $39$ , respectively. The inset in panel (g) zooms in on the green region where  $\lambda \in [0, 0.008]$ .

results in Fig. 4(d). Therefore, the instability time  $\mathcal{T}$  near  $\lambda_c$  scales as  $(\lambda - \lambda_c)^{-1/2}$ .

Figures 4(e)-4(h) show the results for  $N = 21$ , where a pair of  $\rho_j$ s first depart from the unit circle at  $-1$ , indicating a period-doubling bifurcation. Figures 4(i)-4(l) show the results for  $N = 39$ , where a pair of  $\rho_j$ s leave the unit circle as conjugate complex roots, signaling a Hopf bifurcation. Additionally, the results in Figs. 4(g), 4(h), and 4(l) are qualitatively identical, confirming that  $\mathcal{T} \propto (\lambda - \lambda_c)^{-1/2}$ , regardless of the bifurcation type. This conclusion is further supported by the data, including the grey dots in panels (g), (h), and (l). This scaling law matches that of the  $\pi$ -4 mode in the FPUT- $\alpha$  and FPUT- $\beta$  models [36], indicating that the law holds universally across models. Moreover, except for  $N = 9$ , all three types of bifurcations are observed for other values of  $N$ .

Additionally, Figs. 4(e) and 4(g) reveal that  $\lambda_c$  is very small, with  $\Re(\mu_j) > 0$  clearly observable in the inset of Fig. 4(g). Interestingly, the curve of  $\Re(\mu_j) \neq 0$  exhibits an approximately circular shape, suggesting that as  $\lambda$  increases, the system first loses stability and then returns to a stable region (marked by the blue rectangle). As  $\lambda$  continues to rise, the system becomes unstable again, demonstrating a *double instability phenomenon*. Both instability processes are driven by period-doubling bifurcations, as shown in Fig. 5(a), where a pair of  $\rho_j$ s leaves the unit circle from the position of  $-1$  twice.

Figure 5(b) shows  $\Re(\mu_j)$  as a function of  $\lambda$  in a log-log scale. Figure 5(c) presents the MDS results, where

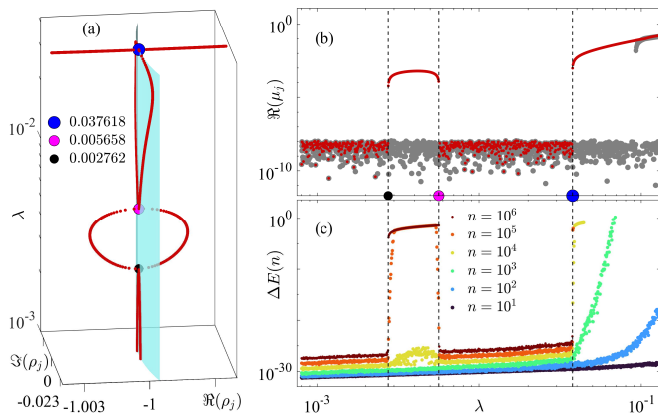


FIG. 5. Panel (a) shows how  $\rho_j$  shifts off the unit circle as  $\lambda$  increases for  $N = 21$ . Panel (b) shows  $\Re(\mu_j)$  versus  $\lambda$ . Panel (c) shows  $\Delta E(n)$  versus  $\lambda$  at different times  $n$ .

$\Delta E(n) = \max \left\{ \sum_{k=1, k \neq 2N/3}^{N-1} E_k(t) \mid t = 1, 2, \dots, n \right\}$ . In the region where  $\Re(\mu_j) > 0$  (here,  $10^{-7}$ ),  $\Delta E$  increases rapidly over time, indicating that the  $\pi/3$ -mode will eventually lose stability. The MDS results align perfectly with the predictions from Floquet theory, as indicated by the vertical lines.

*Summary and discussions*—We have investigated the instability dynamics of the  $\pi/3$ -mode in FPUT- $\alpha$  chains with fixed boundary conditions, leading to four key findings: First, three types of bifurcations—period-doubling, tangent, and Hopf bifurcations—coexist, each triggering instability. Second, we show that the instability time  $\mathcal{T}$  follows a universal scaling law:  $\mathcal{T} \propto (\lambda - \lambda_c)^{-1/2}$ , independent of bifurcation types and models. Third, we find that  $\lambda_c \propto (\tilde{k} - \tilde{k}_c)$ , where  $\tilde{k}_c = 0$  for the Hopf bifurcation regime and  $\tilde{k}_c = \frac{2}{\pi} \arcsin(\frac{\sqrt{3}}{4})$  for the period-doubling regime. Lastly, for certain system sizes (e.g.,  $N = 21$ ), the instability dynamics exhibit a double instability phenomenon, which means that larger perturbations do not necessarily accelerate thermalization.

In the large  $N$  limit, the number of NNMs is small, making the probability of selecting NNMs as the ini-

tial excitation negligible. Additionally, in the period-doubling and Hopf bifurcation regimes, the instability threshold approaches zero as  $N$  increases. Consequently, for large  $N$ , the thermalization dynamics of a generic Hamiltonian system are dominated by multi-wave interactions, resulting in universal thermalization behavior, where the thermalization time is inversely proportional to the square of the perturbation strength [46, 51–59].

However, for finite, especially small  $N$ , the probability of selecting NNMs as the initial excitation increases, and the instability threshold becomes nonzero. In these cases, if the initial excitation corresponds to NNMs, the system exhibits a thermalization threshold: below this threshold, thermalization does not occur, while above it, both instability and multi-wave resonance mechanisms influence the dynamics. As a result, the thermalization time as a function of perturbation strength deviates from simple power-law behavior. Notably, the instability threshold for the tangent bifurcation is finite, leading to a finite threshold behavior in the thermalization dynamics when the initial condition falls within this region.

Our research uncovers a diverse range of destabilization dynamics, which not only deepen the understanding of how the system relaxes to equilibrium but also offer valuable insights into related areas of quantum systems [60], such as the study of (Floquet) time crystals [61–66].

## ACKNOWLEDGMENTS

This work was supported by the National Science Foundation of China (Grants No. 12465010, No. 12247106, No. 12005156, No. 11975190, and No. 12247101). W. Fu also acknowledge support by the Youth Talent (Team) Project of Gansu Province; the Long-yuan Youth Talents Project of Gansu Province; the Project of Fei-tian Scholars of Gansu Province; the Leading Talent Project of Tianshui City; and the Innovation Fund from Department of Education of Gansu Province (Grant No. 2023A-106).

- 
- [1] G. Benenti, G. Casati, and J. Wang, Conservation laws and thermodynamic efficiencies, *Phys. Rev. Lett.* **110**, 070604 (2013).
  - [2] X. Zotos, F. Naef, and P. Prelovsek, Transport and conservation laws, *Phys. Rev. B* **55**, 11029 (1997).
  - [3] B. S. Shastry and A. P. Young, Dynamics of energy transport in a toda ring, *Phys. Rev. B* **82**, 104306 (2010).
  - [4] S. Olla, Role of conserved quantities in Fourier’s law for diffusive mechanical systems, *Comptes Rendus. Physique* **20**, 429 (2019).
  - [5] T. Bountis and H. Skokos, *Complex Hamiltonian Dynamics* (Springer, 2012).
  - [6] P. Y. Lu, R. Dangovski, and M. Soljačić, Discovering conservation laws using optimal transport and manifold learning, *Nat. Commun.* **14**, 4744 (2023).
  - [7] Z. Rieder, J. L. Lebowitz, and E. Lieb, Properties of a harmonic crystal in a stationary nonequilibrium state, *J. Math. Phys.* **8**, 1073 (1967).
  - [8] S. Lepri, R. Livi, and A. Politi, Thermal conduction in classical low-dimensional lattices, *Phys. Rep.* **377**, 1 (2003).
  - [9] A. Dhar, Heat transport in low-dimensional systems, *Adv Phys* **57**, 457 (2008).
  - [10] S. Lepri, *Thermal Transport in Low Dimensions: From Statistical Physics to Nanoscale Heat Transfer*, Lecture Notes in Physics (Springer Cham, 2016).
  - [11] H. Zhao, J. Wang, Y. Zhang, D. He, and W. Fu, Energy transport and diffusion in low-dimensional lattices, *Sci*

- Sin-Phys Mech Astron **51**, 030012 (2021).
- [12] V. I. Arnold, *Mathematical Methods of Classical Mechanics*, 2nd ed., Graduate Texts in Mathematics (Springer New York, NY, 1989) originally published by Nauka, Moscow, 1974.
- [13] E. Fermi, P. Pasta, and S. Ulam, Studies of the nonlinear problems, Los Alamos Scientific Laboratory, Report No. LA-1940 (1955).
- [14] J. Ford, The fermi-pasta-ulam problem: Paradox turns discovery, *Phys. Rep.* **213**, 271 (1992).
- [15] G. Gallavotti, ed., *The Fermi-Pasta-Ulam Problem*, Lecture Notes in Physics, Vol. 728 (Springer Verlag, Berlin, 2008).
- [16] S. Flach, M. V. Ivanchenko, and O. I. Kanakov,  $q$ -breathers and the fermi-pasta-ulam problem, *Phys. Rev. Lett.* **95**, 064102 (2005).
- [17] S. Flach, M. V. Ivanchenko, and O. I. Kanakov,  $q$ -breathers in fermi-pasta-ulam chains: Existence, localization, and stability, *Phys. Rev. E* **73**, 036618 (2006).
- [18] L. Deng, H. Yu, Z. Zhu, W. Fu, Y. Wang, and L. Huang,  $q$ -breathers in the diatomic  $\beta$ -fermi-pasta-ulam- tsingou chains (2024), arXiv:2410.06575 [cond-mat.stat-mech].
- [19] N. Karve, N. Rose, and D. Campbell, Periodic orbits in fermi-pasta-ulam- tsingou systems, *Chaos: An Interdisciplinary Journal of Nonlinear Science* **34**, 093117 (2024).
- [20] H. Christodoulidi, C. Efthymiopoulos, and T. Bountis, Energy localization on  $q$ -tori, long-term stability, and the interpretation of fermi-pasta-ulam recurrences, *Phys. Rev. E* **81**, 016210 (2010).
- [21] T. Kinoshita, T. Wenger, and D. S. Weiss, A quantum newton's cradle, *Nature* **440**, 900 (2006).
- [22] A. Bastianello, A. De Luca, B. Doyon, and J. De Nardis, Thermalization of a trapped one-dimensional bose gas via diffusion, *Phys. Rev. Lett.* **125**, 240604 (2020).
- [23] Y. Le, Y. Zhang, S. Gopalakrishnan, M. Rigol, and D. S. Weiss, Observation of hydrodynamization and local prethermalization in 1d bose gases, *Nature* **618**, 494 (2023).
- [24] L. S. Cao, D. X. Qi, R. W. Peng, M. Wang, and P. Schmelcher, Phononic frequency combs through nonlinear resonances, *Phys. Rev. Lett.* **112**, 075505 (2014).
- [25] A. Mussot, A. Kudlinski, M. Droques, P. Szriftgiser, and N. Akhmediev, Fermi-pasta-ulam recurrence in nonlinear fiber optics: The role of reversible and irreversible losses, *Phys. Rev. X* **4**, 011054 (2014).
- [26] D. Pierangeli, M. Flammini, L. Zhang, G. Marcucci, A. J. Agranat, P. G. Grinevich, P. M. Santini, C. Conti, and E. DelRe, Observation of fermi-pasta-ulam- tsingou recurrence and its exact dynamics, *Phys. Rev. X* **8**, 041017 (2018).
- [27] A. Hudomal, I. Vasić, N. Regnault, and Z. Papić, Quantum scars of bosons with correlated hopping, *Communications Physics* **3**, 99 (2020).
- [28] J. Durnin, M. J. Bhaseen, and B. Doyon, Nonequilibrium dynamics and weakly broken integrability, *Phys. Rev. Lett.* **127**, 130601 (2021).
- [29] N. Darkwah Oppong, G. Pasqualetti, O. Bettermann, P. Zechmann, M. Knap, I. Bloch, and S. Fölling, Probing transport and slow relaxation in the mass-imbalanced fermi-hubbard model, *Phys. Rev. X* **12**, 031026 (2022).
- [30] N. Budinsky and T. Bountis, Stability of nonlinear modes and chaotic properties of 1d fermi-pasta-ulam lattices, *Physica D* **8**, 445 (1983).
- [31] K. Yoshimura, Stability of normal mode oscillations of one-dimensional anharmonic lattices, *Phys. Rev. E* **54**, 5766 (1996).
- [32] S. Flach, Tangent bifurcation of band edge plane waves, dynamical symmetry breaking and vibrational localization, *Physica D: Nonlinear Phenomena* **91**, 223 (1996).
- [33] P. Poggi and S. Ruffo, Exact solutions in the fpu oscillator chain, *Physica D* **103**, 251 (1997).
- [34] G. Chechin, N. Novikova, and A. Abramenko, Bushes of vibrational modes for fermi-pasta-ulam chains, *Physica D* **166**, 208 (2002).
- [35] B. Rink, Symmetric invariant manifolds in the fermi-pasta-ulam lattice, *Physica D* **175**, 31 (2003).
- [36] L. Peng, W. Fu, Y. Zhang, and H. Zhao, Instability dynamics of nonlinear normal modes in the fermi-pasta-ulam- tsingou chains, *New J. Phys.* **24**, 093003 (2022).
- [37] A. Cafarella, M. Leo, and R. A. Leo, Numerical analysis of the one-mode solutions in the fermi-pasta-ulam system, *Phys. Rev. E* **69**, 046604 (2004).
- [38] K. Yoshimura, Modulational instability of zone boundary mode in nonlinear lattices: Rigorous results, *Phys. Rev. E* **70**, 016611 (2004).
- [39] G. Chechin, D. Ryabov, and K. Zhukov, Stability of low-dimensional bushes of vibrational modes in the fermi-pasta-ulam chains, *Physica D* **203**, 121 (2005).
- [40] C. Antonopoulos and T. Bountis, Stability of simple periodic orbits and chaos in a fermi-pasta-ulam lattice, *Phys. Rev. E* **73**, 056206 (2006).
- [41] M. Leo and R. A. Leo, Application of the bogoliubov-krylov method of averaging to the fermi-pasta-ulam system, *Phys. Rev. E* **74**, 047201 (2006).
- [42] C. Antonopoulos, T. Bountis, and C. Skokos, Chaotic dynamics of  $n$ -degree of freedom hamiltonian systems, *Int. J. Bifurcat. Chaos* **16**, 1777 (2006).
- [43] M. Leo and R. A. Leo, Stability properties of the  $n/4$  ( $\pi/2$ -mode) one-mode nonlinear solution of the fermi-pasta-ulam- $\beta$  system, *Phys. Rev. E* **76**, 016216 (2007).
- [44] G. M. Chechin and D. S. Ryabov, Stability of nonlinear normal modes in the fermi-pasta-ulam  $\beta$  chain in the thermodynamic limit, *Phys. Rev. E* **85**, 056601 (2012).
- [45] K. Aoki, Stable and unstable periodic orbits in the one-dimensional lattice  $\phi^4$  theory, *Phys. Rev. E* **94**, 042209 (2016).
- [46] W. Fu, Y. Zhang, and H. Zhao, Universal law of thermalization for one-dimensional perturbed toda lattices, *New J. Phys.* **21**, 043009 (2019).
- [47] See Supplemental Material for additional details on derivation of the solution of  $\pi/3$ -mode, i.e., Eq. (7), and the derivations of Eqs. (10) and (17).
- [48] G. Teschl, *Ordinary differential equations and dynamical systems*, Vol. 140 (American Mathematical Soc., 2012).
- [49] J. Dormand, M. El-Mikkawy, and P. Prince, High-order embedded runge-kutta-nystrom formulae, *IMA J. Numer. Anal.* **7**, 423 (1987).
- [50] Because the reduced wave-number  $\tilde{k} = k/N$ , where  $k \in [1, N/3]$ , in a discrete system, the value of  $\tilde{k}$  is also discrete and constrained by  $N$ .
- [51] W. Fu, Y. Zhang, and H. Zhao, Universal scaling of the thermalization time in one-dimensional lattices, *Phys. Rev. E* **100**, 010101(R) (2019).
- [52] L. Pistone, S. Chibbaro, M. Bustamante, Y. L'vov, and M. Onorato, Universal route to thermalization in weakly-nonlinear one-dimensional chains, *Math. Eng.* **1**, 672 (2019).

- [53] W. Fu, Y. Zhang, and H. Zhao, Nonintegrability and thermalization of one-dimensional diatomic lattices, *Phys. Rev. E* **100**, 052102 (2019).
- [54] Z. Wang, W. Fu, Y. Zhang, and H. Zhao, Wave-turbulence origin of the instability of anderson localization against many-body interactions, *Phys. Rev. Lett.* **124**, 186401 (2020).
- [55] W. Fu, Y. Zhang, and H. Zhao, Effect of pressure on thermalization of one-dimensional nonlinear chains, *Phys. Rev. E* **104**, L032104 (2021).
- [56] S. Feng, W. Fu, Y. Zhang, and H. Zhao, The anti-fermi–pasta–ulam–tsingou problem in one-dimensional diatomic lattices, *J. Stat. Mech. Theory Exp.* **2022**, 053104 (2022).
- [57] M. Onorato, Y. Lvov, G. Dematteis, and S. Chibbaro, Wave turbulence and thermalization in one-dimensional chains, *Phys. Rep.* **1040**, 1 (2023).
- [58] Z. Wang, W. Fu, Y. Zhang, and H. Zhao, Thermalization of two- and three-dimensional classical lattices, *Phys. Rev. Lett.* **132**, 217102 (2024).
- [59] Z. Wang, W. Fu, Y. Zhang, and H. Zhao, Thermalization of one-dimensional classical lattices: beyond the weakly interacting regime, *Commun. Theor. Phys.* **76**, 115601 (2024).
- [60] B. Buča, Unified theory of local quantum many-body dynamics: Eigenoperator thermalization theorems, *Phys. Rev. X* **13**, 031013 (2023).
- [61] F. Wilczek, Quantum time crystals, *Phys. Rev. Lett.* **109**, 160401 (2012).
- [62] V. Khemani, A. Lazarides, R. Moessner, and S. L. Sondhi, Phase structure of driven quantum systems, *Phys. Rev. Lett.* **116**, 250401 (2016).
- [63] J. R. M. de Nova and F. Sols, Continuous-time crystal from a spontaneous many-body floquet state, *Phys. Rev. A* **105**, 043302 (2022).
- [64] J. Jin, L. He, J. Lu, E. J. Mele, and B. Zhen, Floquet quadrupole photonic crystals protected by space-time symmetry, *Phys. Rev. Lett.* **129**, 063902 (2022).
- [65] B. Huang, T.-H. Leung, D. M. Stamper-Kurn, and W. V. Liu, Discrete time crystals enforced by floquet-bloch scars, *Phys. Rev. Lett.* **129**, 133001 (2022).
- [66] M. P. Zaletel, M. Lukin, C. Monroe, C. Nayak, F. Wilczek, and N. Y. Yao, Colloquium: Quantum and classical discrete time crystals, *Rev. Mod. Phys.* **95**, 031001 (2023).